Effects of divertor geometry on H-mode pedestal structure near divertor detachment in the DIII-D tokamak

H. Q. Wang[a], H. Y. Guo, A. W. Leonard, A. L. Moser, T. H. Osborne, P. B. Snyder, E. Belli, R. J. Groebner, D. M. Thomas, J. G. Watkins[b], Z. Yan[c] and the DIII-D group

General Atomics, PO Box 85608, San Diego, CA 92186-5608, USA

[a]*Oak Ridge Associated Universities, Oak Ridge, Tennessee, USA*

[b]*Sandia National Laboratories, PO Box 969, Livermore, CA 94551, USA*

[c]*University of Wisconsin-Madison, Madison, Wisconsin 53706, USA*

E-mail contact: wanghuiqian@fusion.gat.com

Abstract:

Dedicated experiments have been performed in the DIII-D tokamak to assess the influence of divertor geometry on the H-mode pedestal structure. It has been found that in both attached and detached plasmas, compared to the open divertor, the more closed divertor traps more neutrals in the divertor region, leading to lower pedestal fueling and thus results in lower density and higher temperature at the pedestal top. In addition, approaching divertor detachment by increasing the gas-puffing rate, for different divertor geometries, the pedestal width exhibits different trends. In the attached plasma, the pedestal width agrees well with the theoretical and empirical pedestal-poloidal-beta scaling. However, during divertor detachment, in the open divertor the pedestal width is significantly reduced. In contrast, for detached plasmas with the more closed divertor, the pedestal is significantly wider, by up to 50% compared to the theoretical scaling. Moreover, near divertor detachment, the open diverted plasma exhibits a more aligned density and temperature pedestal profile, while in the closed divertor the detachment results in a relative shift (up to 50% of the pedestal width) between the density and temperature pedestal profiles. Such changes in the pedestal structure, coupled with reduced pedestal fueling, allow for the achievement of divertor detachment while retaining high pedestal performance with the more closed divertor.

1. Introduction

The edge pedestal structure of H-mode plasmas remains a critical subject for magnetic fusion plasma research due to the strong impact of the pedestal structure on fusion performance and the potential risk to plasma facing components (PFCs) due to peak ELM heat loads [1-3]. Experiments have found that the divertor and SOL plasma and wall conditions can significantly affect the pedestal structure [4-11]. But it is still not clear how the boundary plasma conditions quantitatively affect the pedestal structure and thus the plasma confinement. In particular, when the plasma approaches divertor detachment, which is essential for the high heat flux operation of future reactor-relevant devices [12-14], more neutrals are ionized near/inside the pedestal, which may greatly affect the pedestal fueling and height. In addition, some experimental results have shown that, although the pedestal width is highly consistent with the EPED model based on the kinetic-ballooning-mode constraint [15-17], the density pedestal position relative to the temperature separatrix is consistent with the neutral penetration model, suggesting the important role of neutrals on the pedestal width [4,5]. Moreover, different divertor conditions can also influence the neutral distribution around the plasma and cause poloidal asymmetry in the scrape-off-layer (SOL) region, which could lead to a strong relative shift of pedestal density and temperature profiles through particle diffusion [6].

Recent experimental and simulation results show that different divertor geometries can change the neutral distribution in the divertor regions [9,18-26,19]. For example, SOLPS modeling [18] shows that compared to an open divertor, a more closed divertor improves the trapping of recycling neutrals, increase the radiative and charge exchange loss in the divertor region, enhance the divertor power dissipation, and thus reduce the divertor plasma temperature and the depositing heat flux. Also confirmed by experiments, a more closed divertor facilitates the achievement of divertor detachment at lower upstream density. Finally SOLPS modeling indicates, in both attached and detached divertor conditions, a more closed divertor prevents recycling neutrals escaping from the divertor region to penetrate into the pedestal region, which may result in less pedestal fueling than an open divertor [9].

In this paper, we will show the significant influence of divertor geometries on the pedestal height, width and displacement between the density and temperature pedestal. When approaching divertor detachment, compared with the open divertor, the H-mode pedestal with more closed divertor shows significantly lower pedestal density, higher pedestal temperature, wider pedestal and significant displacement between the density and temperature pedestal.

2. Experimental setup

Dedicated experiments have been performed in the DIII-D tokamak to study the effect of divertor geometry on divertor detachment and the H-mode pedestal structure. In DIII-D, as illustrated in Fig. 1, the lower divertor physically consists of a flat shelf target plate on the low-field side and vertical target plate on the high-field side. This is a more open divertor. The upper divertor consists of a dome and an outer baffle, which is a more closed divertor. The experiments were conducted in the lower single null configuration and upper single null configuration, respectively. Favorable Bt direction, i.e. lower-single null with ion $B \times \nabla B$ toward the lower X-point and upper single null with ion $B \times \nabla B$ directed to the upper X-point, was chosen to remove the drift effect. In addition, the magnetic geometries were matched as closely as possible, including the elongation, triangularity, q_{95}, and the outer leg of the separatrix.

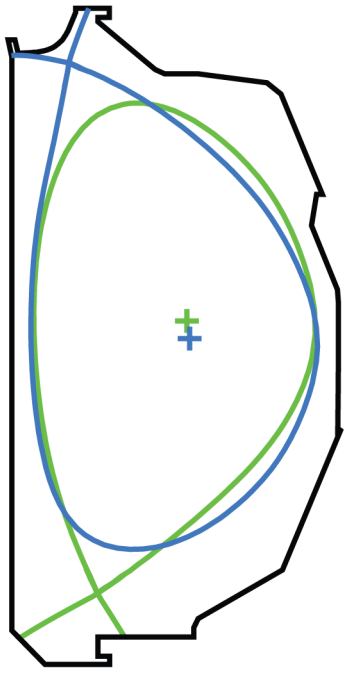

Figure 1. Typical magnetic configuration used in the divertor closure experiment. Note that the upper single null configuration (blue line) is operated in reversed Bt with ion $B \times \nabla B$ upward and the lower single null configuration (green) is operated in forward Bt with $B \times \nabla B$ downward.

Besides the capabilities of the flexible plasma control system, DIII-D is equipped with high spatial and temporal resolution diagnostics [27-29]. The edge electron profiles including electron

density (n_e), temperature (T_e) and pressure (p_e) are measured by a multi-pulse Thomson scattering system, which has a high density of chords spanning the edge transport barrier, and obtains data every several ms throughout the whole plasma discharge. The edge ion temperature and rotation profiles are obtained with a multi-chord charge exchange recombination spectroscopy system oriented along the midplane [27-29]. In order to reduce the scatter of profiles, data are accumulated from the 80-99% of the ELM cycle for many ELMs within specific time windows when the plasma is nearly stationary. The spatial resolution of the pedestal is improved by applying small vertical plasma movements. The experimental data, including the edge temperature, density and pressure profiles, were fit with a modified hyperbolic tangent function (mtanh) to obtain the pedestal heights, widths and gradients that are the key parameters for pedestal studies [27]. Since, from the pedestal to the core region, the gradients of the profiles are still finite, for example, the temperature gradient near the pedestal top could be comparable to that at the pedestal region, we apply the mtanh function to fit the profiles with different radial regions (the one labeled as 'tnh0' for fitting only boundary or near-pedestal profiles and the one labeled as 'tanh' for fitting the whole profiles). All the profile data were mapped to magnetic equilibria so that the fits could be performed as functions of the normalized poloidal magnetic flux coordinate. Due to uncertainties in equilibrium mapping and spatial resolution of the experimental data, adjustment of the separatrix location based on studies with UEDGE and consistent with power flow in the scrape-off layer is made for the profile analysis [27-30]. The locations of T_e, n_e and p_e profiles obtained from Thomson scattering are simultaneously adjusted so that the separatrix is located at one half-width out from the symmetry point of the T_e profile [30].

In this dedicated experiment, density scans were achieved by varying the gas puffing rate discharge by discharge with a fixed gas puffing rate through the entire discharge. To reduce the poloidal asymmetry effects from the gas puffing, the D_2 gas was puffed from a valve under the lower outer baffle at the bottom of machine when running in the USN configuration and behind the upper outer baffle at the top of machine when running in the LSN configuration, respectively. Several diagnostics, i.e. bolometer radiation measurements, tangential TV, IR camera, target Langmuir probes and divertor Thomson scattering, were used to diagnose the divertor conditions. The effect of divertor closure on divertor detachment can be found in Ref. 19.

In this paper, two sets of data with different NBI-heating power, i.e. 3MW and 5MW, are used to examine the effects of divertor closure on the H-mode pedestal structure. In the 3MW cases,

plasma current Ip~1.4MA, toroidal Bt~2T, elongation κ~1.7, triangularity δ~0.58, while in the 5MW cases, Ip~1.3MA, Bt~2T, κ ~1.65, δ~0.54.

3. Pedestal height

Strong gas puffing tends to degrade the pedestal performance in the DIII-D tokamak [13-14] as also reported on other tokamaks [6, 7]. As shown in Fig. 2, with both closed and open divertors and for both 5MW and 3MW cases, increasing the pedestal density by increasing gas-puffing rate reduces both the pedestal temperature and pressure, especially when approaching detachment. It is interesting to note that at a given pedestal density, the pedestal temperatures are similar with both the closed and the open divertors. This may suggest that the pedestal density and temperature, prior to the ELM crash, are strongly coupled, even with different divertor geometries.

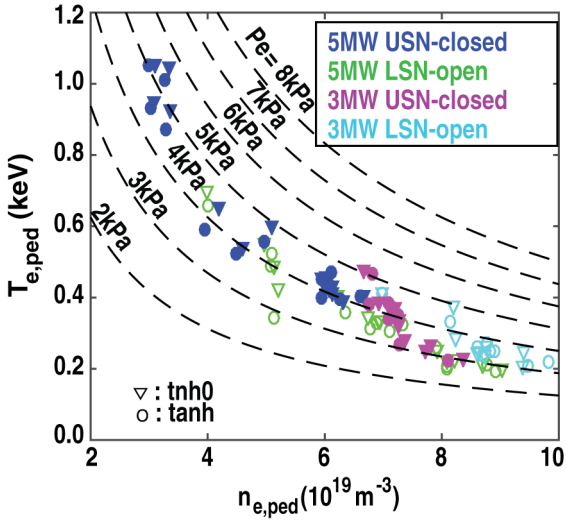

Figure 2. Pedestal top temperature versus pedestal top density in open (open symbols) and closed (filled symbols) divertors. The triangle ones are from the mtanh (modified hyperbolic tangent function) fit for only the near-pedestal region and the circle ones are from mtanh fit for the whole profiles. Four sets of data are shown: 5MW-USN (blue filled symbols), 5MW-LSN (green open symbols), 3MW-USN (pink filled symbols), 3MW-LSN (cyan open symbols). The dash-lines indicate the pedestal pressures at different values.

It is usually found that in the no-gas fuelling case or at the same gas-puffing rate, the pedestal density with the open divertor is much higher than that with the open divertor. The pedestal density at the onset of detachment with the more closed divertor is ~20%-30% lower than that with the open divertor [19]. Hence, the upstream profiles and downstream profiles could not be matched at

the same time for the open and closed divertors. This can be seen by comparing the upstream profiles when the downstream profiles are identical.

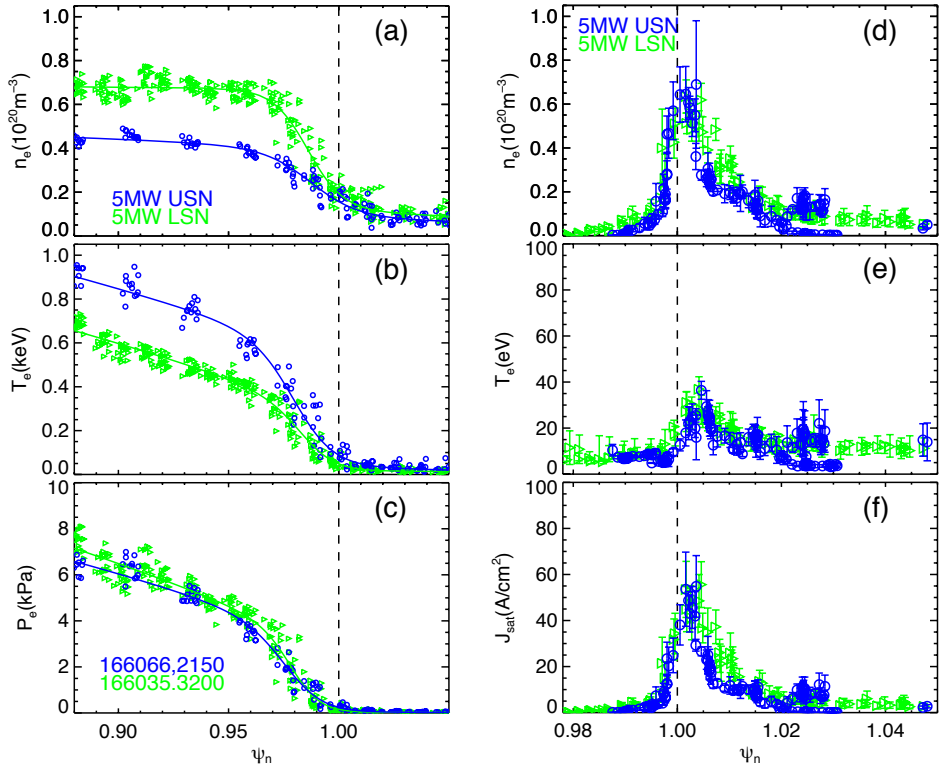

Figure 3. Upstream electron density (a), temperature (b) and pressure (c) profiles measured by the core Thomson scattering system at a similar downstream density (d), temperature (e) and ion saturation current (f) profiles measured by the Langmuir probe embedded in the divertor target plate for two attached discharges with 5MW upper-single null (blue) and 5MW lower-single null (green). Here the target profiles for the closed divertor are radially shift by 0.0015 ψ□ (normalized flux space) to match the peak temperature locations.

Figure 3 compares two cases with the open and closed divertor configurations and nearly matched divertor target profiles, as measured from an array of divertor Langmuir probes. As can be seen, for the attached divertor case, the ion saturation current, as an indicator of the particle flux, peaks near the strike point and the peak temperature is about 35eV, indicating that the divertor plasmas are in the attached state. Note that there is a small (~0.15% ψ□) radial shift of the target profiles between the open and closed divertor, which is probably due to the uncertainty of the magnetic equilibrium. Under this identical attached divertor plasma condition, the pedestal density for the closed divertor configuration is lower by ~30% than that for the open divertor. This is suggestive of lower pedestal fueling in the closed divertor plasma, consistent with results from

SOLPS modeling [9]. The lower pedestal density leads to the higher pedestal temperature. It is also worth pointing out that the pedestal width with the closed divertor is larger than that with the open divertor, but the electron pressures at the pedestal top are similar.

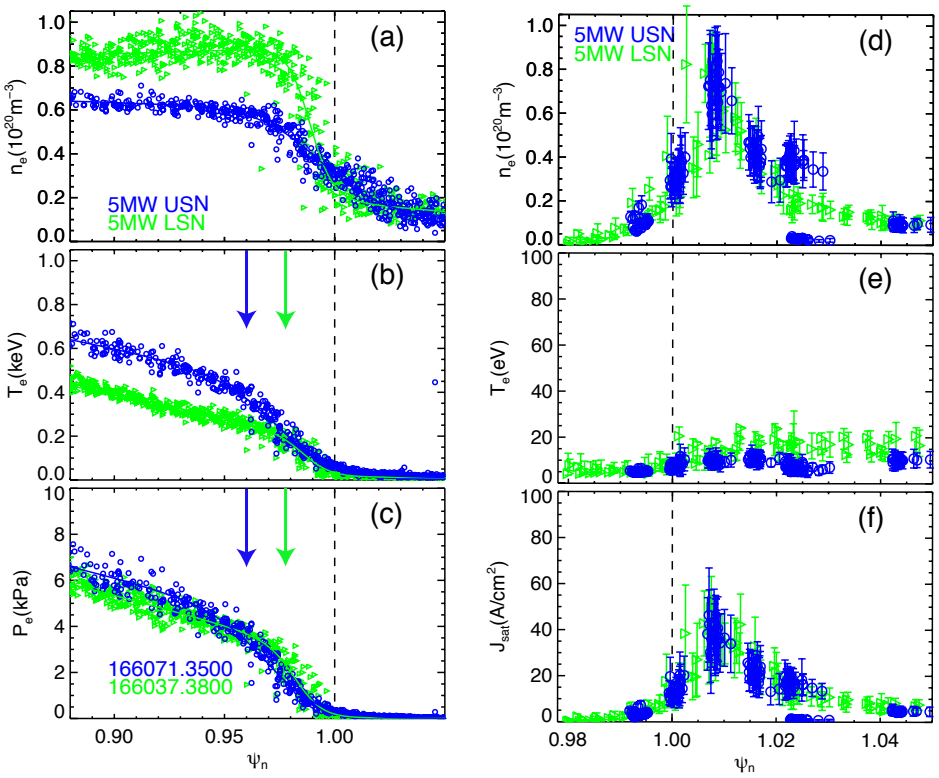

Figure 4. Upstream electron density (a), temperature (b) and pressure (c) profiles measured by the core Thomson scattering system at a similar downstream density (d), temperature (e) and ion current saturation (f) profiles measured by the Langmuir probe embedded in the divertor target plate for two partially detached cases with 5MW upper-single null (blue) and 5MW lower-single null (green) discharge. The locations of density and temperature pedestal top are indicated by the arrow.

In detached plasmas, the more closed divertor also results in lower pedestal fueling, consistent with SOLPS modeling [9]. As shown in Fig. 4, the ion saturation current peaks away the strike point and the electron temperature is low across the SOL, indicating that the divertor plasmas is in the partially detached state, which has also been confirmed by other divertor diagnostics, such as the bolometer radiated power and CII radiation. The pedestal density with the closed divertor is lower than that with the open divertor, while the pedestal temperature is much higher, as observed in the attached plasma cases. In addition, with the closed divertor, the density profile at pedestal is much more flat and extends to the SOL. However, the temperature profiles near the separatrix for the closed divertor almost match those for the open divertor, implying the stiffness of temperature

profile in the steep pressure gradient region [31]. With such stiffness, the pedestal temperature profile is extended further inwardly with the closed divertor, which leads to a much higher temperature at the pedestal top.

4. Pedestal width

As shown in the Fig. 4, both the pedestal height and width in the detached plasmas are significantly different between the open and the closed divertors. It has been found that strong gas puffing can result in some poloidal asymmetry of the density profile in the open-field line region, i.e. SOL region, which may affect the measurements in the SOL [6,32-34]. In DIII-D, as shown in Fig. 4, although there is a higher density near the separatrix in the closed divertor, the density inside the last closed flux surface exhibits a more flat and wider profile. Actually, both the density profile and the temperature profile are much wider in the closed divertor than those in the open divertor.

It is also noted that compared to the closed divertor, for the open divertor the pressure height is much lower in the detached plasmas (Fig.4, the locations of pedestal top are indicated by the arrows), which suggests a lower poloidal pedestal beta $\beta_{p,ped}$ and thus a narrower pedestal width from the $\beta_{p,ped}^{1/2}$ scaling as proposed by the EPED model. The EPED model proposes that the pedestal width is constrained by a critical pressure gradient α_C due to the onset of nearly local kinetic ballooning mode (KBM) turbulence with short wavelengths [15-17]. The EPED modeling predicts that since the normalized pressure gradient $\alpha \propto \frac{\beta_{p,ped}}{\Delta} \propto \frac{1}{s^{1/2}}$ and the magnetic shear s strongly depends on the bootstrap current $s \propto \frac{1}{j} \propto \frac{1}{\beta_{p,ped}}$, this gives a relation $\Delta = c\beta_{p,ped}^{1/2}$. This scaling agrees very well with the experimental empirical scaling from different machines [3, 35], i.e. DIII-D, JET, ASDEX-Upgrade, and in turn, the experimental results from inter-machine comparisons suggest a similar coefficient c~0.076 [35]. Most of the previous comparisons were conducted in attached divertor conditions with few in detached plasmas. To better characterize pedestal width in different divertor conditions and take different pedestal pressures into account, figure 5 compares the normalized pedestal width (average of density and temperature pedestal width) with the empirical scaling.

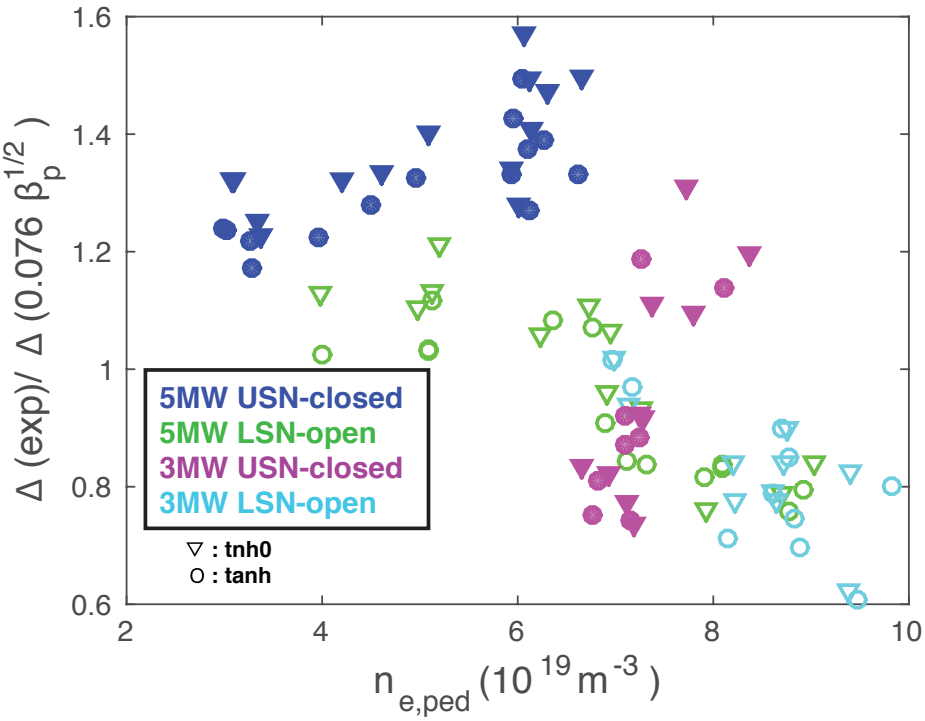

Figure 5. Normalized pedestal width (average of the density and temperature width) to the empirical scaling versus density at pedestal top. Same legends as in Fig. 2: 5MW-USN (blue filled symbols), 5MW-LSN (green open symbols), 3MW-USN (pink filled symbols), 3MW-LSN (cyan open symbols).

As can be seen in Fig. 5, at low density with lower gas puffing and attached divertor plasmas for both different divertor geometries, the experimental pedestal width agrees within 20-30% with the empirical scaling, except the 3MW closed divertor cases. However, by increasing the density to approaching detachment, the experimental pedestal width exhibits different trends for the different divertor geometries. In the more closed diverted plasmas, increasing the pedestal density makes the pedestal wider than the scaling. Especially near the detachment state, experimental profiles can be 50% larger than the scaling. In contrast, in the open diverted plasmas, the pedestal profiles become narrower than the scaling. Especially in detachment at highest density, the pedestal width can be as little as ~60% of the scaling. This narrow pedestal has also been confirmed in other experiments such as the impurity detachment experiments with reversed-Bt, which eliminates the effects of drift and impurity effects. These different trends of pedestal width for the different divertor geometries imply significant influence of divertor conditions on the pedestal besides the kinetic-ballooning-mode constraints.

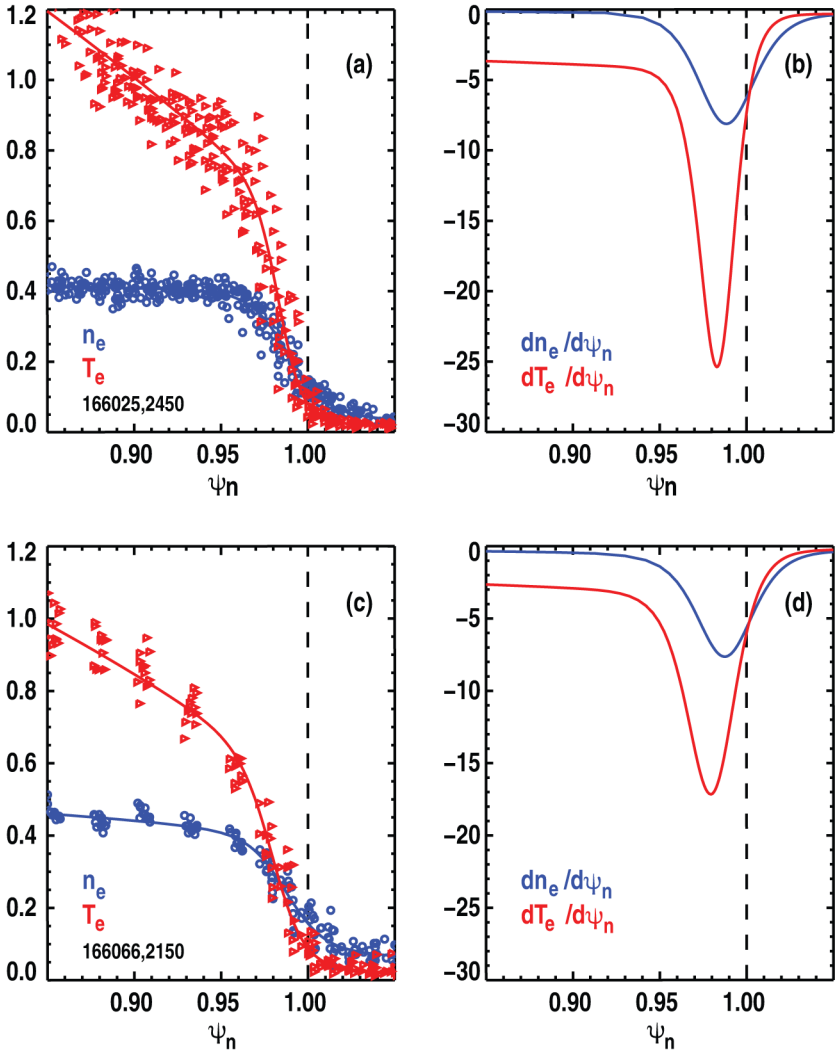

Figure 6. Displacement between steep-gradient regions pedestal density and temperature at a similar pedestal pressure for open and closed divertor plasmas during the attached phase. Open divertor: (a) density profile (blue circle) in $10^{20}m^{-3}$, temperature profile (red triangle) in keV; (b) density gradient (blue), temperature gradient (red). Closed divertor: (c) density profile (blue circle), temperature profile (red triangle); (d) density gradient (blue), temperature gradient (red).

5. Pedestal displacement

Another important comparison between the experimental results and theoretical predictions concerns the displacement between the density and temperature pedestals. The experimental profiles, however, always show a small relative shift between the density and temperature pedestals, especially for the steepest gradient locations. As illustrated in Fig. 6 with attached plasma cases at a similar pedestal density for both open and closed divertors, the peak gradient location of the density pedestal is slightly (<0.5% in normalized flux space) outward of the

temperature pedestal. The peak density gradients in both cases are at similar value, although the temperature gradient in open divertor is higher.

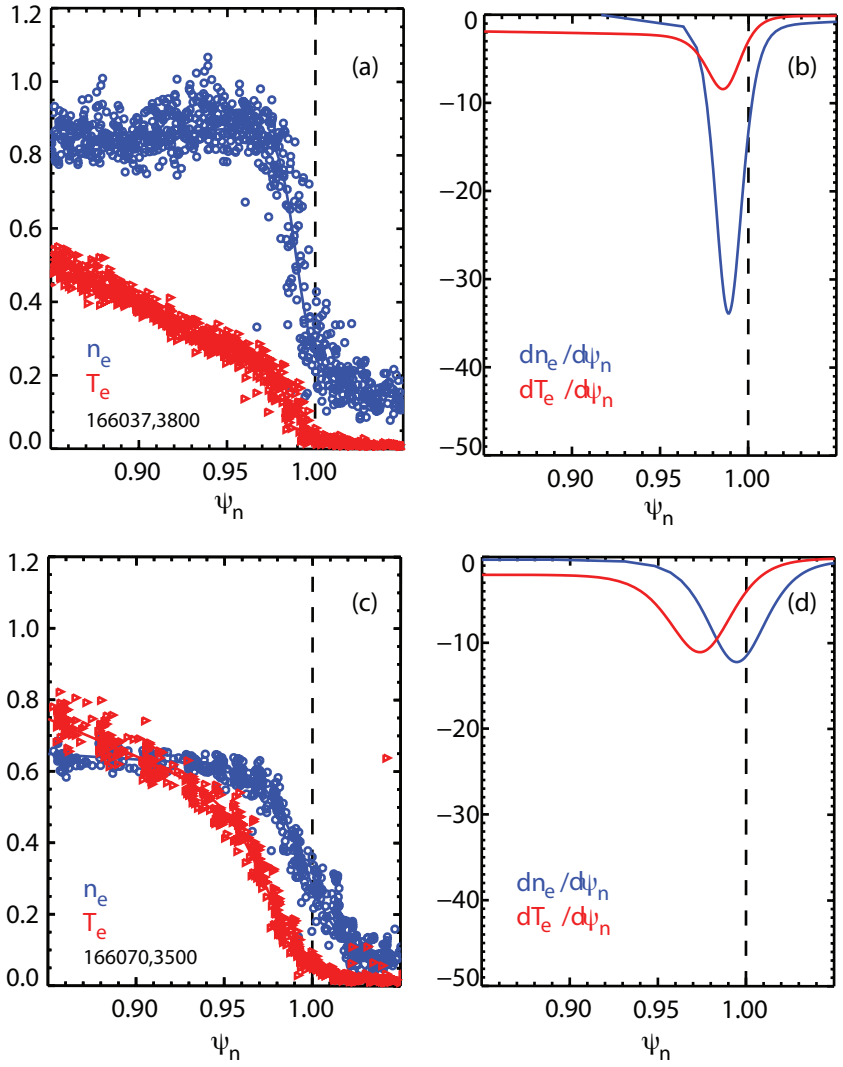

Figure 7. Displacement between the steep-gradient regions pedestal density and temperature in detached plasmas. Open divertor: (a) density profile (blue circle), temperature profile (red triangle); (b) density gradient (blue), temperature gradient (red). Closed divertor: (c) density profile (blue circle), temperature profile (red triangle); (d) density gradient (blue), temperature gradient (red).

However, such a displacement is greatly enhanced in the detached plasma when operating in closed divertor but reduced when operating in open divertor. As shown in Fig. 7, high gas puffing moves the density pedestal radially outward or closer to the separatrix, and cools the plasma near the separatrix, which has also been confirmed in many machines [6,7,13]. The temperature pedestal

also moves towards the separatrix in the open divertor and the displacement remains small. However, in the closed divertor, the divertor detachment doesn't move the temperature pedestal outward or inward very much, and thus results in a relative shift about 2% in ψ_n (~50% of the pedestal width) between the density and temperature pedestal. Not only for the peak gradient location, the pedestal top position also shows similar pedestal displacement (Fig. 7c). In addition, the peak temperature gradients in both divertor geometries are similar, but the peak density gradient with the open divertor is much larger than that with the closed divertor.

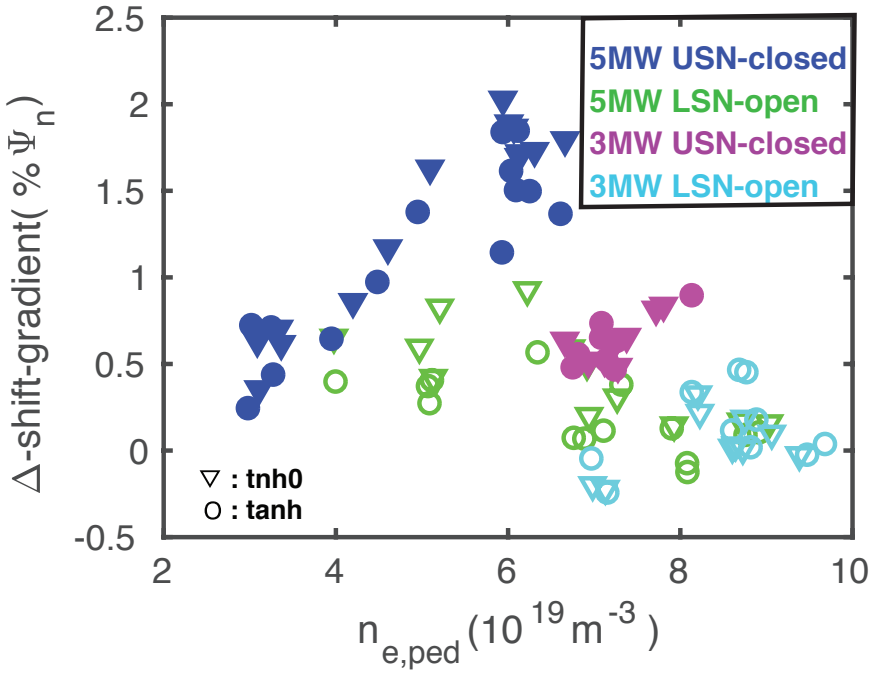

Figure 8. Pedestal displacement versus density at pedestal top. Here we use the relative peak-gradient positions between the density and temperature pedestals. Here, Δ-shift-gradient = $\psi_{ne,mid}$-$\psi_{Te,mid}$, and $\psi_{ne,mid}$ ($\psi_{Te,mid}$) is the position of peak-gradient region of density (temperature) pedestal. Same legends as in the Fig. 2: 5MW-USN (blue filled symbols), 5MW-LSN (green open symbols), 3MW-USN (pink filled symbols), 3MW-LSN (cyan open symbols).

Statistical analysis also exhibits different trends of this displacement approaching detachment by gas puffing, as can be seen in Fig. 8, which is based on the relative peak-gradient positions between the density and temperature pedestal profiles. Here, Δ-shift-gradient = $\psi_{ne,mid}$-$\psi_{Te,mid}$, and $\psi_{ne,mid}$ ($\psi_{Te,mid}$) is the position of peak-gradient region of density (temperature) pedestal. In most of the cases, the density pedestals are slightly outward from the temperature pedestals, which lead to the positive relative shifts. In the open divertor the pedestal displacement is small and tends to

disappear with increasing gas puffing. In the closed divertor, high power and strong gas puffing result in larger displacement between T_e and n_e.

The pedestal top exhibits similar displacement, as shown in Fig. 9. Increasing pedestal density shifts the density pedestal top outwardly, which agrees with neutral penetration model that suggests the neutral penetration and particle transport play important roles on setting the density pedestal profiles [4,5]. In contrast, the locations of temperature pedestal top shows different behavior with increasing density. For the open divertor, increasing density moves the temperature pedestal top outward and reduces the temperature pedestal width, while for the closed divertor, especially in higher power plasmas, the temperature pedestal top locates at nearly same location for both attachment and detachment plasmas. This splitting of the temperature and density pedestal top locations shows a similar displacement as shown in the Fig. 8.

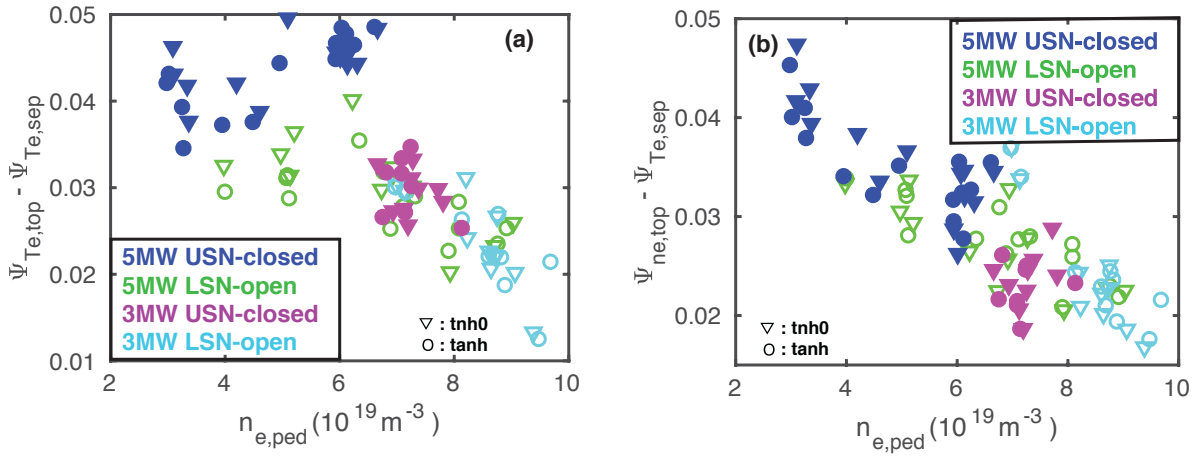

Figure 9. Temperature (a) and density (b) pedestal top relative to the temperature separatrix versus density at pedestal top. Same legends as the Fig. 2: 5MW-USN (blue filled symbols), 5MW-LSN (green open symbols), 3MW-USN (pink filled symbols), 3MW-LSN (cyan open symbols).

Such a strong pedestal displacement may suggest significant decoupling between the particle and thermal transport. One possibility is that the enhanced displacement may drive some extra electron temperature gradient (ETG) driven instabilities. As shown in Fig. 10, the larger relative shift significantly increases the η_e ($\eta_e = L_n/L_{Te}$, where L_n is the density scale length and L_{Te} is the electron temperature scale length at the pedestal steepest pressure gradient region, calculated based on the fitted profiles) which is a critical parameter for the electron temperature gradient mode [36-40]. For the open divertor, η_e is usually not higher than 2 which is near the critical value of ETG mode from simple analytic formulae without considering the flow shear. However, for the

closed divertor, the highest value of η_e is ~3.8, significantly above the critical value of ETG mode. Further effort will be performed to understand the role of the instability on the pedestal structure.

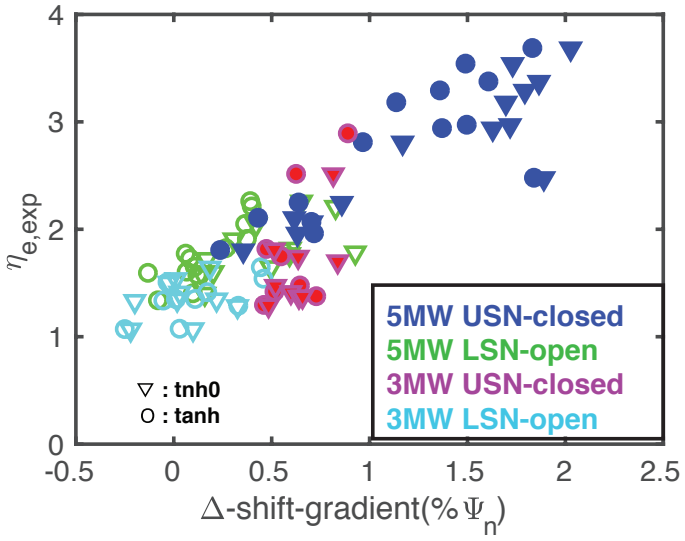

Figure 10. η_e versus pedestal relative shift. Same legends as in Fig. 2: 5MW-USN (blue filled symbols), 5MW-LSN (green open symbols), 3MW-USN (pink filled symbols), 3MW-LSN (cyan open symbols).

6. Instabilities and fluctuations

An important hypothesis in the EPED1 model is that the pedestal height is limited by the onset of non-local peeling-ballooning mode (PBM) at low to intermediate mode number [41-45]. The ELITE code has been implemented to calculate the growth rate of the peeling-ballooning mode prior to the ELM crash. A so-called 'kinetic' equilibria, where the magnetic reconstruction is constrained by pressure profile measurements, is used for the ELITE peeling-ballooing stability calculation. In the kinetic equilibrium, the pressure is taken from the experimental total pressure (including the electron pressure measured by Thomson Scattering, impurity ion pressure measured by CER and estimated main ion pressure, as well as NUBEAM modeled fast ion pressure), the core current profiles are determined from the motional Stark effect (MSE) measurement, the edge current profiles are constrained by a modeled current profile and the plasma shape is determined from the magnetic field and poloidal flux measurements along the vacuum vessel walls [46]. The edge current density profiles are the sum of bootstrap current estimated from the Sauter expression [47], the neutral beam driven current, the Ohmic current which is determined from the neoclassical model, minus a small poloidal current. An iteration was carried out to recalculate the current density and readjust the pressure profiles to match the original experimental profile. To obtain the peeling-

ballooning boundary, a set of equilibria are generated by independently varying pressure and current to provide input into ELITE for separate calculation. A form of diamagnetic stabilization effect derived from BOUT++ calculations was used to determine the stable/unstable boundary [17].

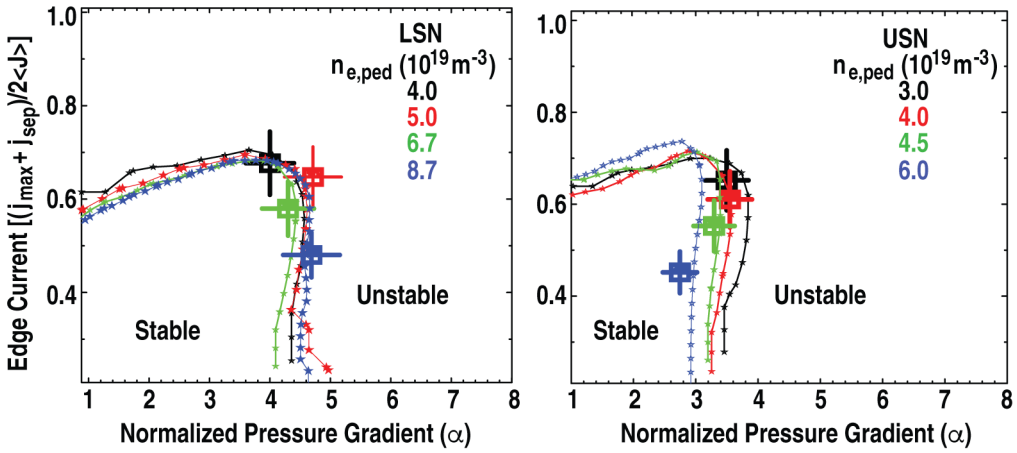

Figure 11. Stability boundary of peeling-ballooning mode from ELITE code calculations in different pedestal density plasmas when operated in open (left) and closed (right) divertors. The boundaries are shown as the star-line. The experimental points with assumed 20% error bar are marked as the bigger square. The highest density cases in these plots are in the detached state and other points are in attached divertor conditions.

The calculated peeling-ballooning stabilities prior to the ELM crash for different densities and different divertor geometries can be found in Fig. 11. All the experimental cases analyzed in this paper are near the peeling-ballooning stability boundary, which agrees with the previous observation of strong coupling between the density and temperature pedestal. Increasing pedestal density does not affect the peeling-ballooning boundary in the open divertor but shifts the boundary slightly inwardly in the closed divertor. Higher pedestal density and thus lower pedestal temperature increases the pedestal collisionality ($\nu^* \propto n_e/T_e^2$), strongly reducing the bootstrap current and gradually moving the peeling-ballooning mode from the medium-n peeling-ballooning-dominant boundary to the high-n ballooning-dominant boundary, usually resulting in a smaller ELM crash. Interestingly, increasing pedestal density slightly increases the normalized pressure gradient in the open divertor and decreases the normalized pressure gradient in the closed divertor, consistent with the different trends in the pedestal width approaching detachment. It should be pointed out that the reduced normalized pressure gradient in the closed divertor does not correspond to a degradation of pedestal performance, since the pedestal is becoming wider and pedestal pressure was not reduced.

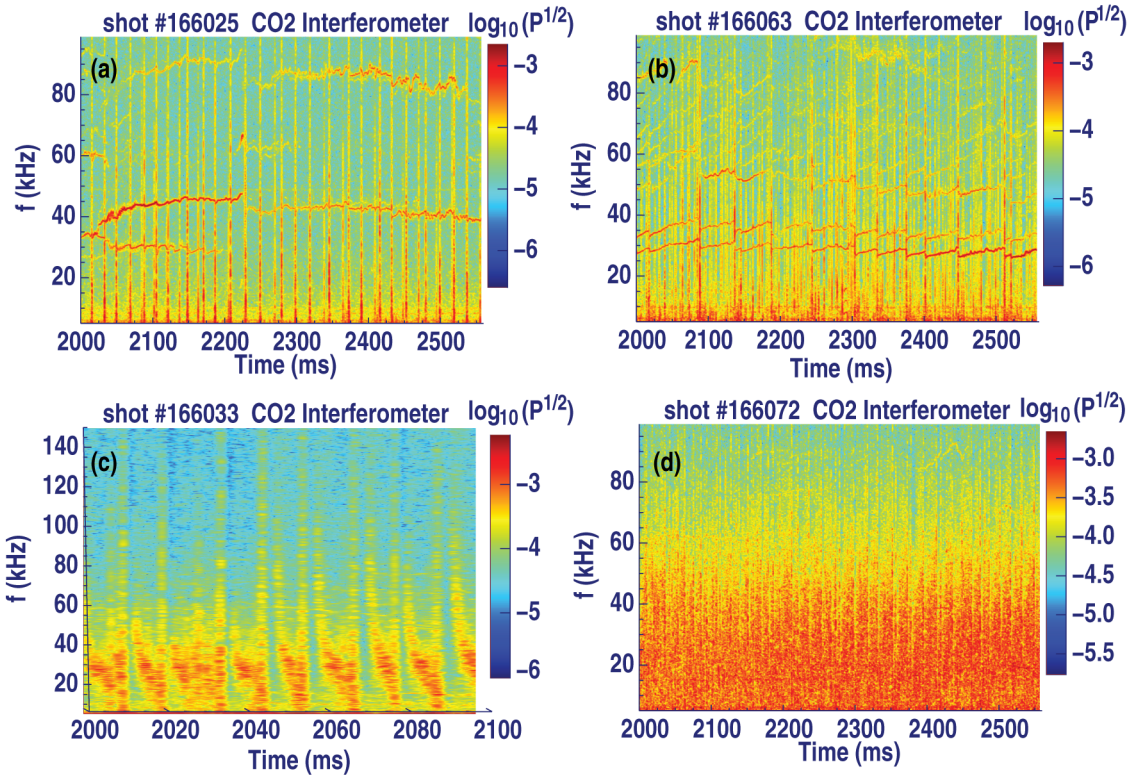

Figure 12. Time-frequency spectrum of fluctuations from CO_2 interferometer measurements for attached LSN (a) and USN (b) and detached LSN (c) and USN (d). The ELMs are shown as bursts in the spectrum. Some core MHD modes which are not related to the ELM crash are seen in the attached plasmas. In the detached plasmas (c-d), some quasi-coherent fluctuations with chirping down frequency from 100kHz to <20kHz are excited and modulated by the ELMs.

It is difficult to calculate the critical limit or growth rate of kinetic-ballooning modes since in the pedestal region the ratio between the gyro-radius and density or temperature gradient length is not small. Instead, as can be seen in Fig. 12, during the inter-ELM phase, some enhanced fluctuations have been observed by pedestal/edge diagnostics, especially near detachment. These fluctuations are modulated by the ELM crashes and are characterized by a sweeping frequency from 100kHz when they are excited after the ELM crash to below ~20kHz when the pedestal saturates prior to the ELM crash. These enhanced fluctuations are different from the core MHD modes that are usually not affected by the ELMs and exhibit nearly constant frequencies in Fig.12 (a-b) with attached plasmas. These enhanced fluctuations exhibit more coherent features in detached plasmas in the open divertor and are much more broadband in the detached closed divertor. In contrast, these fluctuations are very weak and not detectable in attached plasmas.

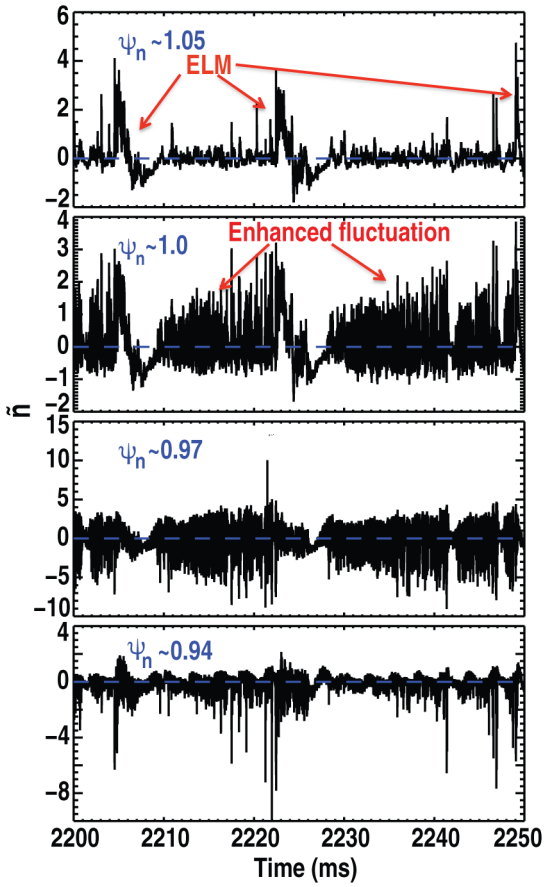

Figure 13. Density fluctuations from BES measurements at different radial locations in/near the pedestal region in detached open divertor plasmas. The ELMs and enhanced fluctuations are shown by the arrow.

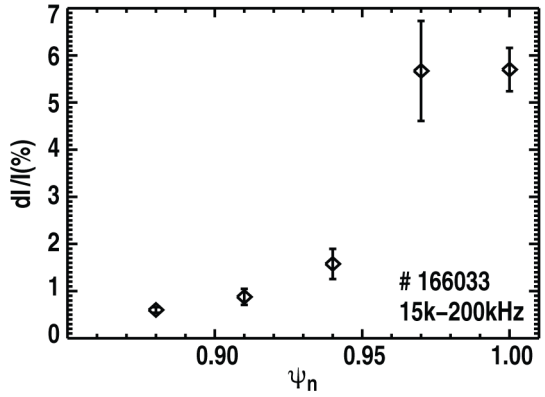

Figure 14. Relative fluctuation level from BES measurement at different radial locations in/near the pedestal region.

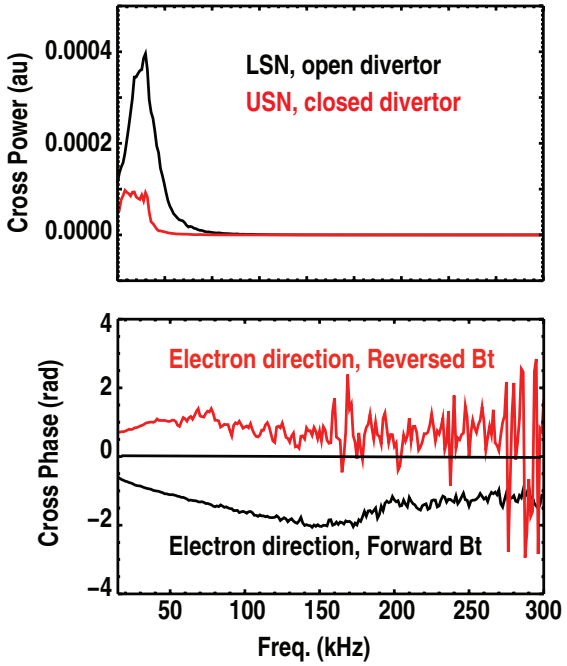

Figure 15. The cross-spectrum and poloidal cross-phase of the density fluctuations from BES measurements in open (black) and closed (red) divertor plasma. The Bt direction is reversed between the LSN and USN, hence the phase delay for electron diamagnetic drift direction is reversed in USN and LSN.

A 2D array of high sensitivity beam emission spectroscopy (BES) covering the whole pedestal region was used to detect the pedestal density fluctuations [48]. From the BES measurements, the enhanced fluctuations peak in the pedestal region and cause a relative fluctuation of about 6% that is nearly one order higher than the background turbulence (Fig. 13 and Fig. 14). It is much weaker in the SOL region or near the pedestal top, suggesting the strong localized characteristic of these enhanced fluctuations. Interestingly these fluctuations exhibit more negative spikes at the inner side of the pedestal and more positive spikes at the foot of the pedestal, similar to blob-hole pair formation, suggesting that the mode may drive outward cross-field transport [19,49,50]. In addition, from BES measurements, as shown in Fig. 15, these enhanced fluctuations propagate in the electron diamagnetic drift direction with poloidal wavelength of about 8-10 cm corresponding a poloidal mode number m > 30. These enhanced fluctuations were not observed on the magnetic probes on the vessel wall, which may be due to the magnetic fluctuation spatial decay at the probe locations.

These enhanced fluctuations show similar mode structures for the open and closed divertor geometries, as can be seen in Fig. 15. Compared to those with the open divertor, for the closed divertor

the fluctuations are weaker, more broadband and at a lower frequency. Future work will be performed to understand the role of such fluctuations on the transport and pedestal structure.

7. Summary

Dedicated experiments in DIII-D have shown strong effects of divertor geometry on the H-mode pedestal structures including the pedestal height, width and displacement between the density and temperature pedestals. In both the attached and detached plasmas, the more closed divertor traps more neutrals in the divertor region and results in lower pedestal fueling, which leads to lower pedestal density and higher pedestal temperature. In addition, as the divertor plasma approaches detachment, the H-mode pedestal width normalized to the pedestal theoretical and empirical $\beta_{p,ped}^{1/2}$ scaling shows different trends between the open and closed divertor geometries. For the open divertor geometry, measurements show that both the density and temperature pedestal widths are strongly reduced during detachment. In contrast, for the closed divertor configuration, the pedestal is significantly wider with a significantly lower pedestal density, especially during detachment, compared to the scaling. This result suggests that neutrals and divertor recycling may have an important effect on the pedestal structure, especially near divertor detachment.

Near divertor detachment, the open diverted plasma exhibits a more aligned density and temperature pedestals, while in the closed divertor the detachment results in a relative shift between the density and temperature pedestals by up to 50% of the pedestal width, which strongly suggests a decoupling between the particle and thermal transport. Other machines such as JET and ASDEX-upgrade have shown that such a strong relative shift could lead to significant degradation of attainable pedestal top pressure [6]. However, in the DIII-D experiments, especially for the closed divertor, the significantly wider pedestal compensates the possible pedestal degradation resulting from the pedestal relative shift, which thus allows for the achievement of higher pedestal performance, i.e. higher pedestal temperature and pressure in detached plasmas than the open divertor case. In addition, the strong relative shift leads to high η_e up to 3.8, which is mainly due to the high temperature gradient and flat density profile at the pedestal region. The flat density profile with high separatrix density would be beneficial for the achievement of divertor detachment. The high temperature gradient would help the achievement of high pedestal performance. Hence, such

a strong relative shift would facilitate the achievement of divertor detachment while retaining high pedestal performance.

Calculations of pedestal stability with the ELITE MHD code for both open and closed divertor configurations, i.e., with either narrower or wider pedestal plasmas, find the plasma profiles right before the ELM crash to be near the predicted peeling-ballooning-mode unstable boundary. Approaching detachment, a strong quasi-coherent mode propagating in the electron-diamagnetic drift direction and driving some outward radial transport is observed from pedestal fluctuation measurements. For the closed divertor configuration with a wider pedestal, these fluctuations appear to be broadband and weaker than that in the open divertor plasmas with a narrower pedestal. Future work will be performed to separate the effects of transport and fueling effects on the pedestal structure.

This work is supported by the U.S. Department of Energy under DE-FC02-04ER54698, DE-AC04-94AL85000 and General Atomics Postdoctoral Research Participation Program administered by ORAU. DIII-D data shown in this paper can be obtained in digital format by following the links at https://fusion.gat.com/global/D3D_DMP. This report was prepared as an account of work sponsored by an agency of the United States Government. Neither the United States Government nor any agency thereof, nor any of their employees, makes any warranty, express or implied, or assumes any legal liability or responsibility for the accuracy, completeness, or usefulness of any information, apparatus, product, or process disclosed, or represents that its use would not infringe privately owned rights. Reference herein to any specific commercial product, process, or service by trade name, trademark, manufacturer, or otherwise does not necessarily constitute or imply its endorsement, recommendation, or favoring by the United States Government or any agency thereof. The views and opinions of authors expressed herein do not necessarily state or reflect those of the United States Government or any agency thereof.

References

[1] ITER Physics Basis Expert Groups on Confinement and Transport and Confinement Modelling and Database, ITER Physics Basis Editors, 1999 *Nucl. Fusion* 39 2175

[2] Doyle E. J. et al 2007 *Nucl. Fusion* 47 S18

[3] Osborne T. H. et al 1998 *Plasma Phys. Control. Fusion* 40 845

[4] Groebner R. J. et al 2004 *Nucl. Fusion* 44 204

[5] Mahdavi M. A. et al 2003 *Phys. Plasmas* 10 3984

[6] Dunne M. G. et al 2017 *Plasma Phys. Control. Fusion* 59 014017

[7] Hughes J. W. et al 2007 *Nucl. Fusion* 47 1057

[8] Fenstermacher M.E. *et al* 2005 *Nucl. Fusion* 45 1493

[9] Sontag A. C. et al 2017 *Nucl. Fusion* 57 076025

[10] Maddison G. P. et al 2014 *Nucl. Fusion* 54 073016

[11] Challis C. D. et al 2015 *Nucl. Fusion* 55 053031

[12] Loarte A. et al 2007 *Nucl. Fusion* 47 S203

[13] Leonard A. W. et al 2015 *J. Nucl. Mater.* 463 519

[14] Leonard A. W. *et al* 2017 *Nucl. Fusion* 57 086033

[15] Snyder P. B. et al 2009 *Phys. Plasmas* 16 056118

[16] Snyder P. B. et al 2009 *Nucl. Fusion* 49 085035

[17] Snyder P. B. et al 2011 *Nucl. Fusion* 51 103016

[18] Sang C. F. et al 2017 *Plasma Phys. Control. Fusion* 59 025009

[19] Moser A.L. et al, APS-DPP 2016

[20] Allen S. L. et al 1999 *Nucl. Fusion* 39 2015

[21] Allen S. L. et al 2001 *J. Nucl. Mater.* 290 995

[22] Fenstermacher M. E. et al 2001 *J. Nucl. Mater.* 290-293 588

[23] Mahdavi M. A. et al 2001 *J. Nucl. Mater.* 290-293 905

[24] Allen S. L. et al 1999 *J. Nucl. Mater.* 266-269 168

[25] Lasnier C. J. et al 1999 *J. Nucl. Mater.* 266-269 577

[26] Groth M. et al 2005 *J. Nucl. Mater.* 337-339 425

[27] Groebner R. J. et al 2009 *Nucl. Fusion* 49 045013

[28] Groebner R. J. et al 2010 *Nucl. Fusion* 50 064002

[29] Osborne T. H. et al 2015 *Nucl. Fusion* 55 063018

[30] Porter G. D. et al 1998 *Phys. Plasmas* 5 1410

[31] Schneider P. A. et al 2013 *Nucl. Fusion* 53 073039

[32] Guimarais L. et al 2018 *Nucl. Fusion* 58 026005

[33] Potzel S. et al 2014 *Nucl. Fusion* 54 013001

[34] Leonard A. W. 2018 *Plasma Phys. Control. Fusion* 60 044001

[35] Beurskens M.N.A. et al 2011 *Phys. Plasmas* 18 056120

[36] Jenko F. et al 2001 *Phys. Plasmas* 8 4096

[37] Ren Y. et al 2011 *Phys. Rev. Lett*. 106 165005

[38] Mazzucato E. et al 2008 *Phys. Rev. Lett*. 101 075001

[39] Coury M. et al 2016 *Phys. Plasmas* 23 062520

[40] Stacey W. M. 2008 *Phys. Plasmas* 15 052503

[41] Snyder P. B. et al 2002 *Phys. Plasmas* 9 2037

[42] Snyder P. B. et al 2004 *Plasma Phys. Control. Fusion* 46 A131

[43] Connor J. W. et al 1998 *Phys. Plasmas* 5 2687

[44] Wilson H. R. et al 1999 *Phys. Plasmas* 6 1925

[45] Wilson H. R. et al 2006 *Plasma Phys. Control. Fusion* 48 A71

[46] Lao L. L. et al 1985 *Nucl. Fusion* 25 1421

[47] Sauter O. et al 1999 *Phys. Plasmas* 6 2834

[48] McKee G. R et al 2010 *Rev. Sci. Instrum.* 81 10D741

[49] Wang H. Q. et al 2014 *Phys. Rev. Lett.* 112 185004

[50] Mazurenko A. et al 2002 *Phys. Rev. Lett.* 89 225004